ACS central science

http://pubs.acs.org/journal/acscii

Research Article

Multielectrode Spectroscopy Enables Rapid and Sensitive Molecular Profiling of Extracellular Vesicles

Tugba Kilic, Young Kwan Cho, Naebong Jeong, Ik-Soo Shin, Bob S. Carter, Leonora Balaj, Ralph Weissleder, and Hakho Lee*

Cite This: *ACS Cent. Sci.* 2022, 8, 110–117

Read Online

ACCESS | Metrics & More | Article Recommendations | Supporting Information

ABSTRACT: Detecting protein markers in extracellular vesicles (EVs) is becoming a useful tool for basic research and clinical diagnoses. Most EV protein assays, however, require lengthy processes—conjugating affinity ligands onto sensing substrates and affixing EVs with additional labels to maximize signal generation. Here, we present an iPEX (impedance profiling of extracellular vesicles) system, an all-electrical strategy toward fast, multiplexed EV profiling. iPEX adopts one-step electropolymerization to rapidly functionalize sensor electrodes with antibodies; it then detects EV proteins in a label-free manner through impedance spectroscopy. The approach streamlines the entire EV assay, from sensor preparation to signal measurements. We achieved (i) fast immobilization of antibodies (<3 min) per electrode; (ii) high sensitivity (500 EVs/mL) without secondary labeling; and (iii) parallel detection (quadruple) in a single chip. A potential clinical utility was demonstrated by directly analyzing plasma samples from glioblastoma multiforme patients.

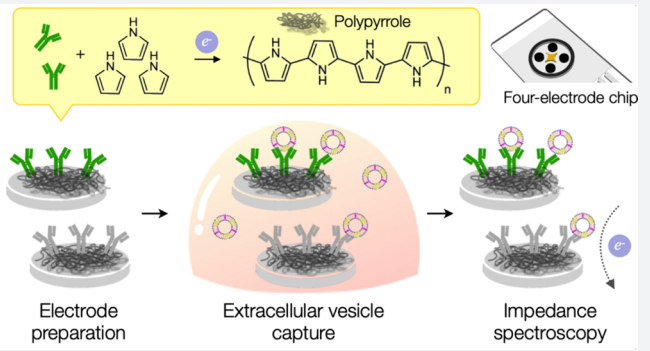

INTRODUCTION

Extracellular vesicles (EVs) have gained traction as a new class of soluble biomarkers. Present in most bodily fluids (e.g., blood, cerebrospinal fluid, urine, saliva), EVs carry molecular constituents of parental tumor and host cells. Analyzing EVs can enable clinicians to detect and monitor tumors in real time, while minimizing complications from specimen collection.[1−3] Profiling EV proteins, in particular, has been shown to achieve high diagnostic accuracy by targeting tumor-specific antigens,[4−6] identify tumor origins or subtypes based on the EV-protein signature,[7−10] and distinguish between indolent and high-risk lesions.[11] New assay formats have been developed to facilitate such EV-protein detection, many of which demonstrated high analytical sensitivity and throughput (see Table S1 for a comparison of methods).[6,12−20] These new systems, however, still have practical limitations in clinical environments: (i) Essentially based on immunodetection, test systems require lengthy preparation steps of immobilizing affinity ligands on sensing devices. (ii) Secondary labeling is often necessary to generate an analytical signal (e.g., sandwich-type assay). (iii) Scaling up assays for parallel multiplexing can be complex.

Here, we present an iPEX (impedance profiling of extracellular vesicles) approach to fast, sensitive, and parallel EV detection. We hypothesized that electrochemistry can be used to streamline the entire EV assay, from sensor preparation to signal measurements. Specifically, we adopted electropolymerization to prime electrodes for target-specific EV capture and electrochemical impedance spectroscopy for label-free EV detection. Electropolymerization enables fast, one-step deposition of polymers on electrodes.[21,22] We applied the method to rapidly immobilize antibodies on a custom-designed iPEX chip. Furthermore, through a selective application of electrical potential, multiple electrodes were individually functionalized, each with antibodies against a different protein target; the prepared iPEX chip allowed for parallel detection of multiple markers. For subsequent EV assays, we used an iPEX chip to capture EVs and measured changes in electrochemical impedance. The iPEX approach offered the advantages of (i) fast immobilization of antibodies (<3 min) on electrodes; (ii) high sensitivity (~500 EVs/mL) without the need for a secondary labeling; and (iii) multimarker detection in a single chip. As a pilot clinical application, we used iPEX to directly analyze plasma samples from healthy donors (n = 10) and glioblastoma (GBM) patients (n = 10).

Received: September 29, 2021
Published: January 7, 2022

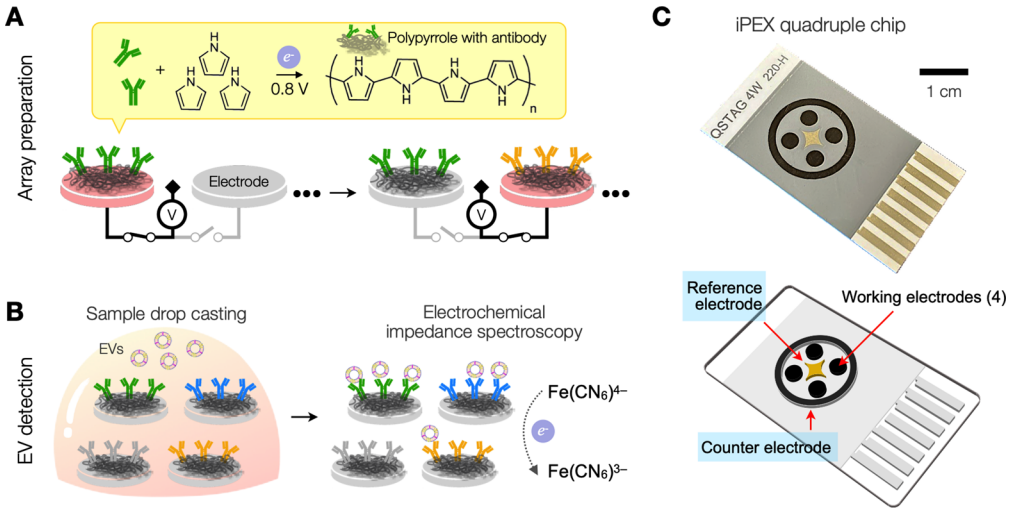

Figure 1. iPEX strategy. (A) Surface functionalization. A mixture of antibodies and pyrrole was drop-cast onto electrodes. Performing cyclic voltammetry coated a select electrode with antibodies through electrochemical polymerization. The process was repeated for other electrodes with new pyrrole−antibody mixtures. (B) Label-free detection of extracellular vesicles (EVs). An EV sample was loaded over functionalized electrodes, and the electrochemical impedance of each electrode was measured using a ferri- and ferrocyanide couple as a redox probe. (C) An iPEX chip for quadruple measurements was custom-designed. Four working electrodes (carbon) were individually addressed during measurements, whereas the reference electrode (Ag/AgCl) and the counter electrode (carbon) were shared.

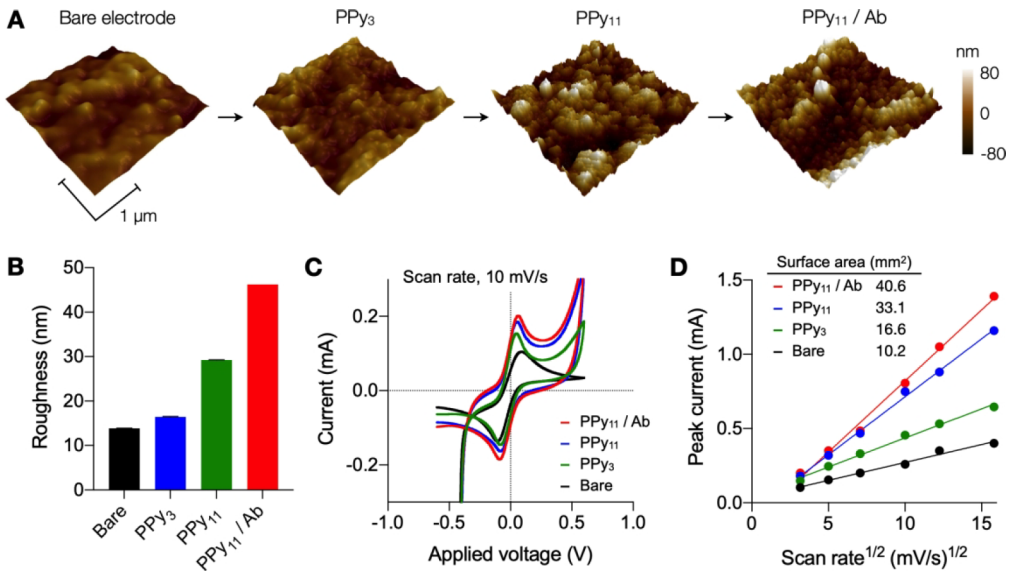

Figure 2. Characterization of sensor electrodes. (A) Atomic force microscopy was used to investigate the surface of bare and polypyrrole (PPy)-coated electrodes. (B) The surface roughness increased, as the polymerization was repeated and antibodies were incorporated. PPy_3 and PPy_{11}, 3 and 11 polymerization cycles, respectively; PPy_{11}/Ab, 11 polymerization in the presence of antibody (Ab). (C) Cyclic voltammograms of different electrode conditions were recorded at the presence of ferri- and ferrocyanide. The non-Faradaic current increased with repeated polymerization, indicating the gradual thickening of the PPy layer. (D) The peak current was measured, while the potential scan rate was varied in cyclic voltammetry. From the measured data, the effective reaction area was estimated for the ferri- and ferrocyanide redox process (inset). Note the increase of reaction area with polymerization and antibody embedding.

RESULTS AND DISCUSSION

iPEX Strategy. Figure 1 summarizes the iPEX workflow. To prepare sensors for EV detection, we immobilized capture antibodies on the electrode surface through simple electropolymerization (Figure 1A). A mixture of antibodies and pyrrole (Py) monomers was added to a given electrode, and an electrical potential was applied to induce a polymerization reaction (see the Experimental Section for details).[22] During Py polymerization into polypyrrole (PPy), antibodies were entrapped in the polymer matrix. For EV profiling, we flood-loaded samples over an electrode array to target-specifically capture EVs on individual electrodes (Figure 1B). Captured EVs changed the charge transfer resistance of the electrochemical reaction, which was measured via impedance spectroscopy. To further increase the resistance signal, antibodies against tetraspanins (e.g., CD63, CD9, or CD81), which are overexpressed in EVs, could be introduced as an optional, secondary label.

The iPEX approach simplified the sensor preparation for immunoassays. We could rapidly (3 min) functionalize electrodes with antibodies in one simple step rather than relying on chemical conjugation. Importantly, antibodies

https://doi.org/10.1021/acscentsci.1c01193
ACS Cent. Sci. 2022, 8, 110−117

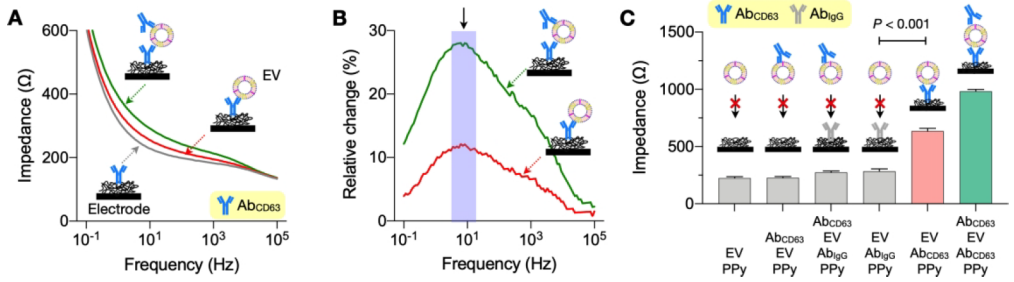

Figure 3. iPEX assay optimization. (A) Bode impedance plots during assay steps. As EVs were captured and further labeled with additional antibodies, electrochemical impedance values gradually increased between 10 and 1000 Hz. (B) Relative impedance changes against background (no EVs) had their maxima around 10 Hz which was set as the iPEX detection frequency. (C) Impedance values were measured from different assay conditions. Significant signal changes occurred only when electrodes were configured for target-specific EV capture. Data were obtained at 10 Hz and displayed as mean ± SD from quadruplicate measurements.

against different protein targets can be selectively immobilized on designated electrodes. The polymerization occurs only in an electrode connected to a potentiostat while other unconnected electrodes remain unmodified. The following EV assays were also facilitated with samples applied to all electrodes in a single drop fashion. To take these advantages, we custom-designed an iPEX chip for parallel processing (Figure 1C). Four detection spots (working electrodes) were arranged as a circular array, and they shared common reference and counter electrodes that were placed in a symmetrical way. This arrangement made the chip compact and minimized the number of required electrical contacts. The iPEX chip was fabricated on a flexible substrate with electrodes patterned through screening printing (Experimental Section).

Surface Characterization. We first characterized the formation of PPy and antibody entrapment on electrodes. The topography of electrode surfaces, measured by atomic force microscopy, indicated that surface roughness increased with cycles of electropolymerization (Figure 2A,B). Py-polymerization with antibodies further increased surface roughness (Figure 2B), suggesting antibody embedding.

Cyclic voltammetry confirmed the change in polymer thickness as well as antibody entrapment in the polymer matrix (Figure 2C and Figure S1). Using electrodes that had different polymerization conditions, we measured electrochemical redox behavior of 10 mM $K_3(FeCN)_6$ in 100 mM KCl aqueous solution, at the scan rate of 10 mV/s. Ferricyanide is a typical redox species exhibiting one-electron, quasireversible oxidation. A bare carbon electrode showed an oxidation anodic peak at the applied voltage of E_{pa} = 103 mV and a reversal cathodic peak at E_{pc} = −109 mV (against the reference electrode). The peak current ratio was ∼0.8 indicating quasireversible redox conversion between $[Fe(CN)_6]^{3-}$ and $[Fe(CN)_6]^{4-}$ at $E_{1/2}$ = −3 mV (= $[E_{pa} + E_{pc}]/2$). As PPy progressively covered the electrode surface, the non-Faradaic current increased, indicating the capacitive charging/discharging through the PPy layer. We set the Py-polymerization cycle to 11. Further increasing the cycle number led to no appreciable changes in voltammograms, suggesting a limiting behavior.

We further estimated the effective surface area of PPy-coated electrodes by measuring voltammograms at different scan rates (ν = 10, 25, 50, 100, 150, and 250 mV/s). The oxidation peak current (i_p) was then fitted to the Randles−Sevcik equation (Figure 2D):

$$i_p = 2.69 \times 10^5 S D^{1/2} n^{3/2} C \nu^{1/2} \quad [A]$$

where S is the surface area (cm^2), D is the diffusion coefficient (7.66×10^{-6} cm^2/s for $[Fe(CN)_6]^{3-}$),[23] n is the number of electrons transferred (n = 1), and C is the total concentration of electroactive species (mol/cm^3). The effective surface area of the electrode increased with PPy coating and antibody entrapment (Figure 2D, inset); the results qualitatively matched with roughness measurements and with a previous report.[24]

Assay Optimization. We next optimized the iPEX assay for EV detection. We measured electrochemical impedance (Z) of three assay steps (Figure 3A, Figure S2), before EV capture on an electrode, after EV capture, and postlabeling for signal amplification. The impedance spectra had three general features: (i) At high frequency (>10^4 Hz), the Z value converged to electrolyte resistance, as the electrochemical reaction became diffusion limited. (ii) Between 10 and 10^4 Hz, impedance differences emerged, driven by the electrical resistance at the electrode−electrolyte interface. (iii) Below 10 Hz, the double-layer capacitance became dominant, and impedance differences disappeared. The impedance change after EV capture was maximal near 10 Hz (Figure 3B) which was set as the iPEX detection frequency.

We further compared EV-specific and background signals (Figure 3C). When electrodes were not configured for EV capture (i.e., PPy matrices without capture antibodies or with nonspecific IgG control antibodies), iPEX reported low impedance upon incubation with EV samples (GLI36 EVs; 10^5 EVs/mL, 200 μL). The measured Z values were slightly higher with PPy-IgG electrodes than with PPy-only electrodes, which can be attributed to antibody entrapment in the polymer. With electrodes functionalized with CD63 antibodies, the impedance rose significantly from the background (P < 0.001; two-sided t-test) and could be further increased through the secondary labeling. These results demonstrated target-specific EV capture with iPEX electrodes, indicating that antibodies embedded in PPy retained their affinity.

For EV detection, we measured two Z values, one from a capture electrode (Z_M) and the other from an IgG control electrode (Z_{IgG}). As an analytical metric, we used the net difference ($\Delta Z_M = Z_M - Z_{IgG}$). This differential metric allowed us to compensate for signals coming from nonspecific EV binding. We also placed the IgG control site per chip to monitor potential chip-to-chip variations (Figure S3).

iPEX Performance. Applying the optimized protocol, we next characterized iPEX's performance for EV detection. To examine selectivity in multiplexed detection, we prepared a set of iPEX chips with varying assignments of EV targets (i.e.,

https://doi.org/10.1021/acscentsci.1c01193
ACS Cent. Sci. 2022, 8, 110−117

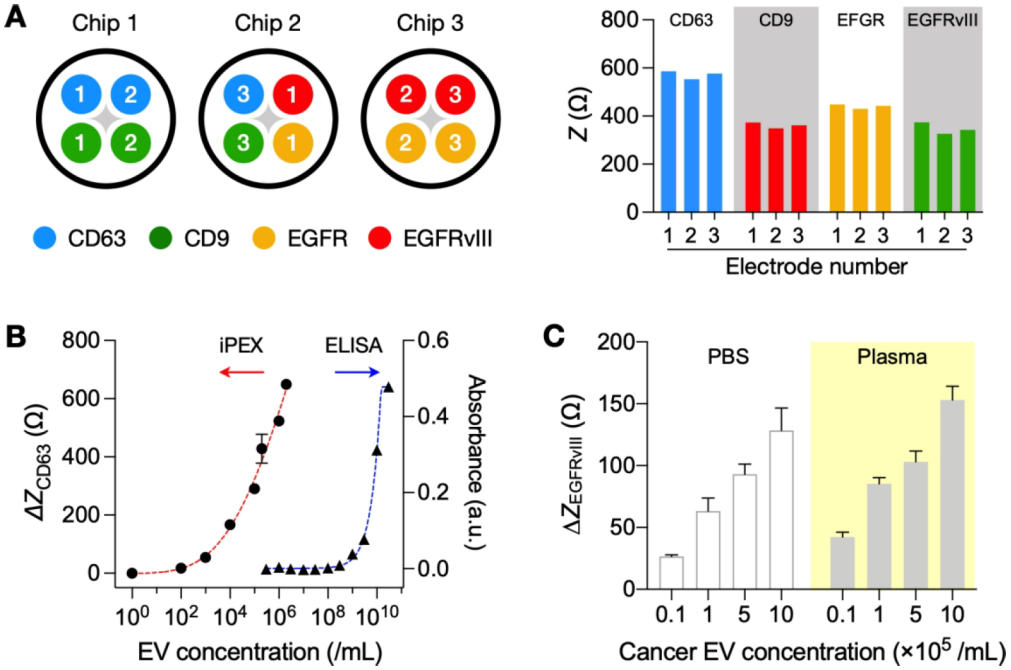

Figure 4. iPEX assay performance. (A) Potential cross-talk between electrodes was assessed. Three different iPEX chips were configured to detect CD63, CD9, EGFR, or EGFRvIII (color-coded in the left schematic). The bar graph on the right shows measured impedance values. Electrode positions are color-coded and numbered. (B) Comparison of detection sensitivity. Samples containing varying amounts of EVs in phosphate-buffered saline (PBS) were analyzed by iPEX and enzyme-linked immunosorbent assay (ELISA). EVs were probed for CD63 expression. For iPEX, the limit of detection was close to 500 EV/mL, and the dynamic range spanned up to 5 orders of magnitude. For ELISA, the limit of detection was about 10^8 EV/mL. Data are shown as mean ± SD from technical duplicates. (C) Cancer EVs (GLI36vIII cells) were spiked in PBS and human serum and assayed by iPEX for EGFRvIII. The analytical resolution of iPEX was comparable in both media. Data are shown as mean ± SD from quadruplicate measurements.

CD63, CD9, EGFR, or EGFRvIII) among electrodes (Figure 4A, left); each chip was functionalized to detect at least two different protein markers. EV samples (from 10^4 EVs/mL; GLI36 cell line) were drop-loaded to cover electrodes, and electrochemical impedance was measured. For a given protein target, we observed consistent Z values (coefficient of variation <7%) regardless of electrode assignment (Figure 4A, right). The results confirmed (i) the immobilization of target antibodies only on intended electrodes during Py polymerization and (ii) negligible electrical crosstalk between electrodes.

We next determined iPEX's detection sensitivity. Samples with varying EV concentrations were prepared and detected via CD63-specific iPEX chips. The label-free iPEX achieved a limit of detection (LOD) of ∼500 EVs/mL and a dynamic range of 5 orders of magnitude (Figure 4B). The observed LOD was much lower than those of ELISA (∼10^8 EV/mL) and was comparable to or better than those by other EV profiling technologies (see Table S1 for comparison). We further tested whether plasma samples could be directly used without purification. Samples were prepared by spiking EVs (from GLI36vIII cells) into PBS or plasma. We then detected EGFRvIII to exclude the endogenous signal from plasma EVs. Plasma samples showed Z values that were slightly higher than those for samples in buffer (Figure 4C). Abundant plasma proteins apparently adsorbed on electrodes to raise the background level. In both media, however, the net signal changes were similar between different EV concentrations (Figure S4), which indicated that iPEX retained analytical resolution.

Profiling of Clinical GBM Samples. To demonstrate its clinical utility, we tuned iPEX to detect GBM-derived EVs (see Figure S5 for the study design). We first used a panel of GBM cell lines (GLI36, GLI36vIII, U87, U87vIII, GBM 11/5, GBM R132H) for marker validation.[5,25,26] Flow cytometry (Figure 5A) on these cells revealed differential expression of EGFR, EGFRvIII, and PDGFRα. These markers have been shown to be unregulated in GBM. *EGFR* gene overexpression has been reported in up to 57% of GBM cases, followed by *PDGFRα* (13%).[27] EGFRvIII is highly GBM-specific and the most common EGFR mutation in GBM.[28,29] Using iPEX, we next screened cell-derived EVs for these GBM markers. The marker profiles of EVs positively correlated with those of parent cells (Pearson r = 0.78; Figure 5B), which supported EV's utility as a tumor surrogate.

We next pilot-tested iPEX with human plasma samples. Clinical samples (n = 20) were collected from healthy controls (n = 10) and GBM patients (n = 10; see Table S2 for patient information). We used a pair of iPEX chips for a given plasma sample: a tetraspanin chip whose four electrodes were functionalized for CD63, CD9, CD81, and IgG (control), respectively; and a GBM chip whose four electrodes were functionalized for known GBM markers (EGFR, EGFRvIII, PDGFRα) and IgG (control). The tetraspanin chip was used to estimate EV loading for signal normalization. For GBM markers, we normalized the measured impedance values (ΔZ_{GBM}) against ΔZ_{CD63} (from the tetraspanin chip), defining $Z_{norm} = \Delta Z_{GBM}/\Delta Z_{CD63}$; this metric was used to account for different EV concentrations among samples.

Figure 5C summarizes the profiling results. The top heatmap (Figure 5C, top) shows impedance values (ΔZ) from the

https://doi.org/10.1021/acscentsci.1c01193
ACS Cent. Sci. 2022, 8, 110−117

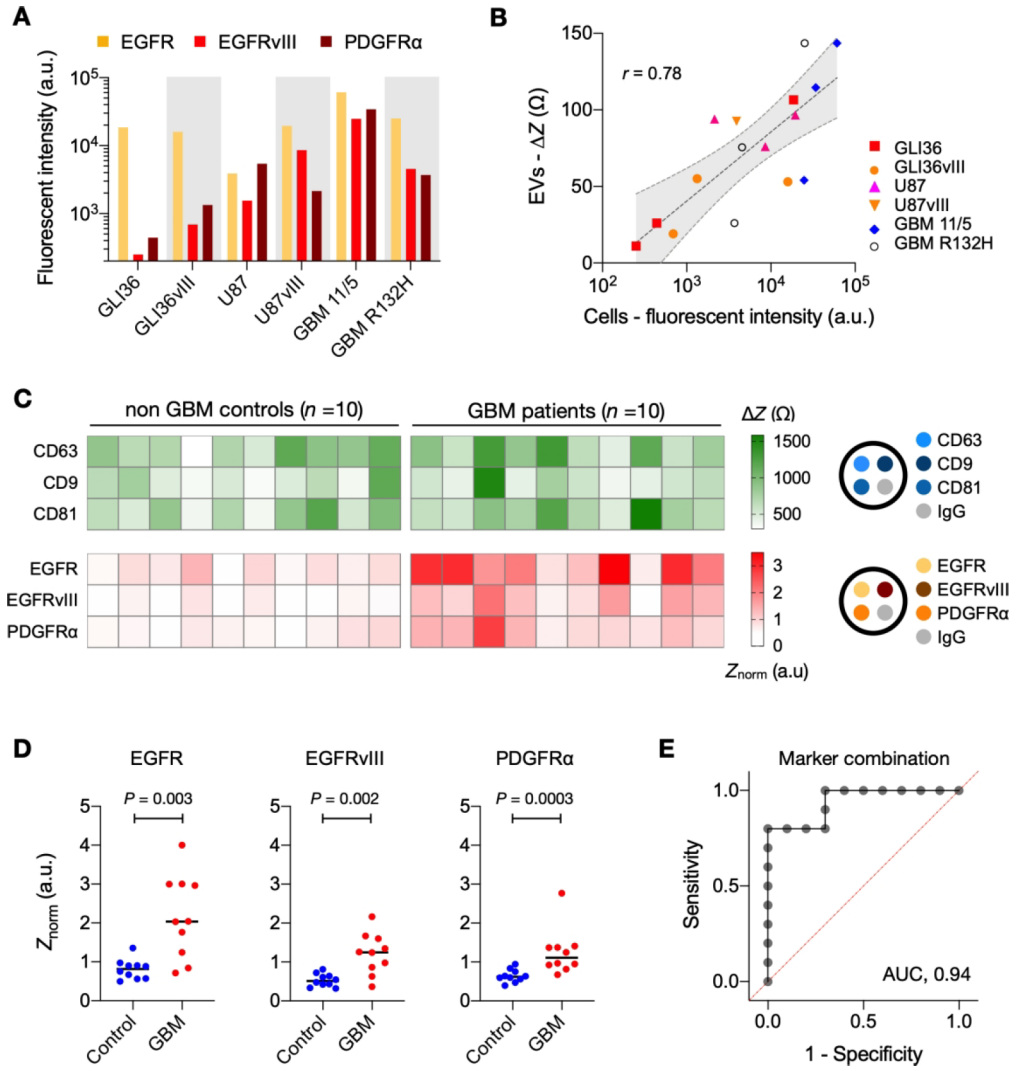

Figure 5. GBM EV detection. (A) A panel of GBM cell lines were profiled via flow cytometry to validate the expression of key GBM protein markers (EGFR, EGFRvIII, PDGFRα). a.u., arbitrary unit. (B) iPEX was applied to detect GBM markers in cell-line-derived EVs. Expression profiles correlated between EVs and cells (Pearson correlation coefficient, r = 0.78), supporting EVs' use as a cellular surrogate. (C) Plasma EVs from GBM patients (n = 10) and healthy controls (n = 10) were profiled for EV-specific tetraspanins (CD63, CD9, CD81) and GBM markers (EGFR, EGFRvIII, PDGFRα). The inset (right) shows the marker assignment for tetraspanin and GBM chips. Impedance values from tetraspanin measurements (ΔZ_M, M = CD63, CD9, CD81) were nondiagnostic with no significant difference between patient and control groups. (D) GBM markers, when normalized against EV load ($Z_{norm} = \Delta Z_{GBM}/\Delta Z_{CD63}$), were elevated in the patient cohort. (E) Expressions of three GBM markers were combined through logistic regression, and a receiver operation characteristic curve was constructed for GBM diagnostics. The area under the curve (AUC) via iPEX EV profiling was 0.94.

tetraspanin (CD63, CD81, CD9) measurements. Tetraspanin levels showed high variations with no significant difference between controls and GBM patients (Figure S6). On the other hand, the normalized expression (Z_{norm}) of GBM markers (Figure 5C, bottom) was observed as higher in GBM patients (Figure 5D). We further estimated the diagnostic power of each GBM marker by constructing receiver operating characteristic (ROC) curves (Figure S7). The areas under the curve (AUCs) were 88% (EGFR), 90% (EGFRvIII), and 92% (PDGFR). Combining three markers improved the AUC to 94% (Figure 5E).

CONCLUSIONS

The iPEX approach simplified and sped up EV protein assays. By codepositing affinity ligands through electropolymerization, iPEX rapidly and selectively primed sensors specific to target proteins. The following EV assays measured electrochemical impedance that is highly responsive to the sensor surface, which allowed iPEX to achieve excellent sensitivity (~500 EVs/mL). The assay was performed in a label-free manner. No additional antibody binding was necessary to generate an analytical signal; this advantage simplified and sped up the assay procedure, contrasting with conventional sandwich-type assays (e.g., ELISA). We prototyped a quadruplex iPEX chip and tuned it to detect key GBM markers (i.e., EGFR, EGFRvIII, PDFGRa). With one-drop loading of a plasma sample, iPEX detected multiple EV protein markers, which led to high diagnostic accuracy in classifying GBM from noncancer cases. Further validation, however, would be necessary to test the specificity of these markers in differentiating GBM from other tumor types. iPEX can facilitate such studies by allowing for high-throughput, multiple-marker assays.

https://doi.org/10.1021/acscentsci.1c01193
ACS Cent. Sci. 2022, 8, 110−117

We expect that the iPEX assay would be more sensitive in detecting small EVs and other smaller targets such as exomeres, cytokines, and serum proteins. These targets can bind to electrodes at a high density, which would lead to large changes in charge transfer impedance (ΔZ). More importantly, small targets can shorten the assay time due to favorable kinetics. The required time (τ) to capture the detection target on an electrode scales as $\tau \sim 1/(Da)$, where D is the diffusivity of the target, and a is the diameter of an electrode.[30] Because D is inversely promotional to the hydrodynamic size (d_h) of the target, we estimate that $\tau \sim d_h/a$. For typical EVs ($d_h \sim 150$ nm), our assay time was $\tau_{EV} \sim 60$ min. With smaller targets, for example, antibodies ($d_h \sim 10$ nm), this time would be in the order of a few minutes (60 min ×10/150).

We also envision other technical developments to improve iPEX's analytical capabilities. First, one could enhance the throughput by implementing an array of microelectrodes. Each electrode would still be functionalized via selective electropolymerization, obviating the need for external microprinting of reagents. Using such arrays would reduce the sample volume (to cover electrodes) while increasing the number of markers analyzed. Second, a new measurement device could be designed for electrode arrays. An appealing approach is to use a common potentiostat but configure it to sequentially access individual electrodes. Because measuring impedance at a single frequency is fast (<0.1 s), this configuration will effectively realize a parallel detection in a compact device. With these improvements, iPEX would be a powerful, microarray-type platform, facilitating comprehensive EV-protein profiling for clinical diagnoses.

EXPERIMENTAL SECTION

Multielectrode Design and Fabrication. The quadruple iPEX chip was designed to have four individual working electrodes, one counter electrode, and one reference electrode. Electrodes were fabricated via screen printing (QSTAG, Korea). A carbon ink and a Ag/AgCl paste were screen-printed for working/counter and reference electrodes, respectively, on a flexible poly(ethylene terephthalate) substrate (thickness, 1 mm). The chip was then partly covered with an insulating layer and heat-treated for 1 h. The final fabricated chip had a cross-shaped Ag/AgCl reference electrode (area, 5.3 mm^2) in the center, four circular working electrodes (diameter, 3 mm), and a ring-shaped counter electrode.

Electrode Functionalization. Pyrrole (reagent grade, 98%, Sigma-Aldrich) solution (0.1 M) was prepared in 0.1 M NaCl supporting electrolyte. The antibody (Ab) of interest (see Table S3) was diluted in pyrrole solution to a final concentration of 6 μg/mL. Electropolymerization of pyrrole to polypyrrole (PPy) was performed via cyclic voltammetry between 0.0 and +0.95 V with respect to the Ag/AgCl reference electrode at the scan rate of 50 mV/s. After polymerization, electrodes were washed with phosphate-buffered saline (PBS) buffer and kept in PBS until use. The surface topography of electrodes was measured using an atomic force microscope (NX-10, Park Systems) equipped with CONTSCR cantilevers (NanoWorld). Topography images were generated using XEI software (Park Systems).

iPEX Detection. EV samples (200 μL) were drop-cast on PPy-Ab functionalized electrodes and incubated for 1 h at 20 °C. For optional signal amplification, CD63 antibody (2 μg/mL) was drop-cast on captured EVs and incubated for 1 h at 20 °C. A potentiostat with an impedance analyzer (Sp-200, Bio-Logic) was used to perform electrochemical impedance spectroscopy. The electrolyte was a mixture of $K_4[Fe(CN)_6]$ (10 mM) and $K_3[Fe(CN)_6]$ (10 mM) in a phosphate (50 mM)-buffered K_2SO_4 (100 mM) solution (pH 7). The impedance spectrum was measured over a frequency range from 100 mHz to 100 kHz with a 10 mV alternative current voltage superimposed on a constant bias of −0.195 V.

Enzyme-Linked Immunosorbent Assay (ELISA). CD63 antibody and IgG antibody were diluted in PBS (5 μg/mL) and added to the Maxisorp 96-well plate (Nunc) for overnight incubation at 4 °C. After washing with PBS, 2% bovine serum albumin (BSA) in PBS was added to the plate (2 h incubation at 20 °C). For EV detection, samples (in 100 μL of PBS) were added to each well for 1 h of incubation at 20 °C. After discarding samples, biotinylated CD63 antibody (1 μg/mL) was added to each well and incubated for another 2 h at room temperature (RT). Unbounded antibodies were removed via triple-washing with PBS. Streptavidin-HRP molecules then were added to each well, and the mixture was incubated for 1 h at 20 °C. After washout with PBS, a solution of chromogenic electron mediator (3,3′,5,5′-tetramethylbenzidine) was added. After 20-min incubation, a stop solution (2 M, H_2SO_4) was added. The optical density at 450 nm was then read by a plate reader (Tecan).

GBM Cell Culture. GLI36 and U87-EGFR cell lines were purchased from ATTC. GLI36vIII and U87vIII cell lines were generated from GLI36 and U87-EGFR cell lines, respectively, through lentivirus transduction.[26] GBM 11/5 and GBM R132H primary cell lines were obtained from Dr. Breakefield's laboratory (Massachusetts General Hospital). All cell lines were cultured in Dulbecco's modified essential medium (DMEM, Life Technologies) that contained 10% fetal bovine serum (FBS; Thermo Fischer Scientific) and 1% penicillin/streptomycin (10 IU/mL and 10 μg/mL, respectively; Thermo Fischer Scientific).

EV Isolation from Cell Culture. Cells at passage 1−20 were cultured until 80% confluency in their complete medium and then in DMEM containing 5% depleted FBS for 48 h. Next, the conditioned media from ∼10^7 cells were collected, filtered through a 0.2 μm filter (Millipore), and centrifuged at 300g for 10 min. The supernatant was concentrated to 0.5 mL via a centrifugal filter (Centricon Plus-70 centrifugal filter 10 kDa cutoff) and added to a qEV 70 nm column (iZon). As the supernatant passed through the column, 4 mL of PBS was added in 100−200 μL aliquots. First, 3 mL was discarded, and a subsequent 1.5 mL was collected as an EV fraction. As a final step, EVs were concentrated with an Amicon Ultra-2 centrifugal filter unit with an Ultracel-100 membrane. The size and concentration of prepared EVs were measured via nanoparticle-tracking analysis (LM10, Melvern).

Flow Cytometry. About 10^5 cells were used per marker for flow cytometry. Cells were fixed with 4% formaldehyde (ThermoFisher) in PBS for 15 min at room temperature on a nutating mixer. Fixed cells were then washed twice in PBS−BSA (1× PBS with 0.5% BSA) and incubated with primary antibodies (10 μg/mL) in PBS−BSA for 1 h at room temperature. Labeled cells were washed twice in PBS−BSA, incubated with fluorophore-conjugated secondary antibodies (1:1000 dilution) for 30 min at room temperature, and washed again. Control samples were similarly labeled using isotype-matched IgG and secondary antibodies. The fluorescence signal was measured using a CytoFlex flow cytometer

https://doi.org/10.1021/acscentsci.1c01193
ACS Cent. Sci. 2022, 8, 110−117

(Beckman Coulter) with 96-well plate handling. A total of 10 000 events were collected. The expression level of a target marker was calculated as the signal difference between targeted and control samples.

Clinical Samples. The study population included patients 18 years or older with pathology confirmed gliomas who underwent surgery at the Massachusetts General Hospital and age-matched healthy controls. For glioma cohorts, exclusion criteria consisted of a history of other primary or metastatic cancers, active infectious disease, current or previous enrollment in clinical trials, and hemolyzed plasma samples. All healthy control subjects were screened for pertinent oncologic and neurologic medical histories. Individuals with a history of cancer, neurological disorders, and infectious diseases were excluded from the study. All samples were collected with written informed consent after the patient was advised of the potential risks and benefits, as well as the investigational nature of the study. Our studies were conducted in accordance with principles for human experimentation as defined in the U.S. Common Rule and were approved by the Human Investigational Review Board of each study center under Partners institutional review board (IRB)-approved protocol number 2017P001581. Caution! Clinical samples should be handled following Biosafety Level (BSL) 2 protocols. PPy-Ab functionalized electrodes were directly incubated with plasma samples (100 μL) for 1 h at room temperature, and the iPEX signal was measured after washing the electrodes with PBS twice.

■ ASSOCIATED CONTENT

Supporting Information

The Supporting Information is available free of charge at https://pubs.acs.org/doi/10.1021/acscentsci.1c01193.

> Scan rate study; functionalization and selectivity test; chip reproducibility; sensitivity comparison; GBM detection workflow; expression of tetraspanins in EVs; receiver operation characteristic (ROC) analyses; comparison of EV protein detection methods; patient demographics information; and antibodies used in this study (PDF)

■ AUTHOR INFORMATION

Corresponding Author

Hakho Lee − *Center for Systems Biology, Massachusetts General Hospital, Boston, Massachusetts 02114, United States; Department of Radiology, Massachusetts General Hospital, Harvard Medical School, Boston, Massachusetts 02114, United States;* orcid.org/0000-0002-0087-0909; Email: hlee@mgh.harvard.edu

Authors

Tugba Kilic − *Center for Systems Biology, Massachusetts General Hospital, Boston, Massachusetts 02114, United States; Department of Radiology, Massachusetts General Hospital, Harvard Medical School, Boston, Massachusetts 02114, United States*

Young Kwan Cho − *Center for Systems Biology, Massachusetts General Hospital, Boston, Massachusetts 02114, United States; Department of Chemistry, Kennedy College of Sciences, University of Massachusetts Lowell, Lowell, Massachusetts 01854, United States*

Naebong Jeong − *Center for Systems Biology, Massachusetts General Hospital, Boston, Massachusetts 02114, United States*

Ik-Soo Shin − *Department of Chemistry, Soongsil University, Seoul 06978, South Korea;* orcid.org/0000-0001-6344-4176

Bob S. Carter − *Department of Neurosurgery, Massachusetts General Hospital, Harvard Medical School, Boston, Massachusetts 02114, United States*

Leonora Balaj − *Department of Neurosurgery, Massachusetts General Hospital, Harvard Medical School, Boston, Massachusetts 02114, United States*

Ralph Weissleder − *Center for Systems Biology, Massachusetts General Hospital, Boston, Massachusetts 02114, United States; Department of Radiology, Massachusetts General Hospital, Harvard Medical School, Boston, Massachusetts 02114, United States; Department of Systems Biology, Harvard Medical School, Boston, Massachusetts 02115, United States*

Complete contact information is available at: https://pubs.acs.org/10.1021/acscentsci.1c01193

Notes

The authors declare no competing financial interest.

■ ACKNOWLEDGMENTS

The authors thank Dr. Breakefield (Massachusetts General Hospital) for helpful discussion. This work was supported in part by U.S. NIH Grants P01CA069246 (R.W.), R01CA229777 (H.L.), R21DA049577 (H.L.), R01CA204019 (R.W.), U01CA233360 (H.L.), P01CA069246 (B.S.C.), R01CA239078 (B.S.C., H.L.), R01CA237500 (B.S.C., H.L.), and U01CA230697 (B.S.C., L.B.); US DOD-W81XWH1910199 (H.L.) and DOD-W81XWH1910194 (H.L.); and MGH Scholar Fund (H.L.). T.K. is grateful to the Swiss National Science Foundation for the Postdoc Mobility fellowship (P400PM_180788/1).

■ REFERENCES

(1) Skog, J.; Würdinger, T.; van Rijn, S.; Meijer, D. H.; Gainche, L.; Sena-Esteves, M.; Curry, W. T.; Carter, B. S.; Krichevsky, A. M.; Breakefield, X. O. Glioblastoma Microvesicles Transport RNA and Proteins That Promote Tumour Growth and Provide Diagnostic Biomarkers. *Nat. Cell Biol.* **2008**, *10* (12), 1470−1476.

(2) Nilsson, J.; Skog, J.; Nordstrand, A.; Baranov, V.; Mincheva-Nilsson, L.; Breakefield, X. O.; Widmark, A. Prostate Cancer-Derived Urine Exosomes: A Novel Approach to Biomarkers for Prostate Cancer. *Br. J. Cancer* **2009**, *100* (10), 1603−1607.

(3) Xu, R.; Rai, A.; Chen, M.; Suwakulsiri, W.; Greening, D. W.; Simpson, R. J. Extracellular Vesicles in Cancer - Implications for Future Improvements in Cancer Care. *Nat. Rev. Clin. Oncol.* **2018**, *15* (10), 617−638.

(4) Park, J.; Park, J. S.; Huang, C.-H.; Jo, A.; Cook, K.; Wang, R.; Lin, H.-Y.; Van Deun, J.; Li, H.; Min, J.; et al. An Integrated Magneto-Electrochemical Device for the Rapid Profiling of Tumour Extracellular Vesicles From Blood Plasma. *Nat. Biomed. Eng.* **2021**, *5* (7), 678−689.

(5) Shao, H.; Chung, J.; Balaj, L.; Charest, A.; Bigner, D. D.; Carter, B. S.; Hochberg, F. H.; Breakefield, X. O.; Weissleder, R.; Lee, H. Protein Typing of Circulating Microvesicles Allows Real-Time Monitoring of Glioblastoma Therapy. *Nat. Med.* **2012**, *18* (12), 1835−1840.

(6) Im, H.; Shao, H.; Park, Y. I.; Peterson, V. M.; Castro, C. M.; Weissleder, R.; Lee, H. Label-Free Detection and Molecular Profiling

of Exosomes With a Nano-Plasmonic Sensor. *Nat. Biotechnol.* **2014**, *32* (5), 490−495.
(7) Liu, C.; Zhao, J.; Tian, F.; Cai, L.; Zhang, W.; Feng, Q.; Chang, J.; Wan, F.; Yang, Y.; Dai, B.; et al. Low-Cost Thermophoretic Profiling of Extracellular-Vesicle Surface Proteins for the Early Detection and Classification of Cancers. *Nat. Biomed. Eng.* **2019**, *3*, 183−193.
(8) Rontogianni, S.; Synadaki, E.; Li, B.; Liefaard, M. C.; Lips, E. H.; Wesseling, J.; Wu, W.; Altelaar, M. Proteomic Profiling of Extracellular Vesicles Allows for Human Breast Cancer Subtyping. *Commun. Biol.* **2019**, *2*, 325.
(9) Dong, H.; Chen, H.; Jiang, J.; Zhang, H.; Cai, C.; Shen, Q. Highly Sensitive Electrochemical Detection of Tumor Exosomes Based on Aptamer Recognition-Induced Multi-DNA Release and Cyclic Enzymatic Amplification. *Anal. Chem.* **2018**, *90* (7), 4507−4513.
(10) Liu, C.; Zhao, J.; Tian, F.; Cai, L.; Zhang, W.; Feng, Q.; Chang, J.; Wan, F.; Yang, Y.; Dai, B.; et al. Low-Cost Thermophoretic Profiling of Extracellular-Vesicle Surface Proteins for the Early Detection and Classification of Cancers. *Nat. Biomed. Eng.* **2019**, *3*, 183−193.
(11) Yang, K. S.; Lin, H. Y.; Curley, C.; Welch, M. W.; Wolpin, B. M.; Lee, H.; Weissleder, R.; Im, H.; Castro, C. M. Bead-Based Extracellular Vesicle Analysis Using Flow Cytometry. *Adv. Biosyst.* **2020**, *4* (12), No. e2000203.
(12) Jeong, S.; Park, J.; Pathania, D.; Castro, C. M.; Weissleder, R.; Lee, H. Integrated Magneto-Electrochemical Sensor for Exosome Analysis. *ACS Nano* **2016**, *10* (2), 1802−1809.
(13) Lee, K.; Fraser, K.; Ghaddar, B.; Yang, K.; Kim, E.; Balaj, L.; Chiocca, E. A.; Breakefield, X. O.; Lee, H.; Weissleder, R. Multiplexed Profiling of Single Extracellular Vesicles. *ACS Nano* **2018**, *12* (1), 494−503.
(14) Duijvesz, D.; Versluis, C. Y. L.; van der Fels, C. A. M.; Vredenbregt-van den Berg, M. S.; Leivo, J.; Peltola, M. T.; Bangma, C. H.; Pettersson, K. S. I.; Jenster, G. Immuno-Based Detection of Extracellular Vesicles in Urine as Diagnostic Marker for Prostate Cancer. *Int. J.* **2015**, *137* (12), 2869−2878.
(15) López-Cobo, S.; Campos-Silva, C.; Moyano, A.; Oliveira-Rodríguez, M.; Paschen, A.; Yáñez-Mó, M.; Blanco-López, M. C.; Valés-Gómez, M. Immunoassays for Scarce Tumour-Antigens in Exosomes: Detection of the Human Nkg2d-Ligand, Mica, in Tetraspanin-Containing Nanovesicles From Melanoma. *J. Nanobiotechnology* **2018**, *16* (1), 47.
(16) Kowal, E. J. K.; Ter-Ovanesyan, D.; Regev, A.; Church, G. M. Extracellular Vesicle Isolation and Analysis By Western Blotting. *Methods Mol. Biol.* **2017**, *1660*, 143−152.
(17) Silvers, C. R.; Miyamoto, H.; Messing, E. M.; Netto, G. J.; Lee, Y. F. Characterization of Urinary Extracellular Vesicle Proteins in Muscle-Invasive Bladder Cancer. *Oncotarget* **2017**, *8* (53), 91199−91208.
(18) Kilic, T.; Valinhas, A. T. S.; Wall, I.; Renaud, P.; Carrara, S. Label-Free Detection of Hypoxia-Induced Extracellular Vesicle Secretion From MCF-7 Cells. *Sci. Rep.* **2018**, *8* (1), 9402.
(19) Mathew, D. G.; Beekman, P.; Lemay, S. G.; Zuilhof, H.; Le Gac, S.; van der Wiel, W. G. Electrochemical Detection of Tumor-Derived Extracellular Vesicles on Nanointerdigitated Electrodes. *Nano Lett.* **2020**, *20* (2), 820−828.
(20) Jørgensen, M.; Bæk, R.; Pedersen, S.; Søndergaard, E. K. L.; Kristensen, S. R.; Varming, K. Extracellular Vesicle (Ev) Array: Microarray Capturing of Exosomes and Other Extracellular Vesicles for Multiplexed Phenotyping. *J. Extracell. Vesicles* **2013**, *2* (1), 20920.
(21) Berkes, B. B.; Bandarenka, A. S.; Inzelt, G. Electropolymerization: Further Insight Into the Formation of Conducting Polyindole Thin Films. *J. Phys. Chem. C* **2015**, *119* (4), 1996−2003.
(22) Sabouraud, G.; Schottland, P.; Sadki, S.; Brodie, N. The Mechanisms of Pyrrole Electropolymerization. *Chem. Soc. Rev.* **2000**, *29* (5), 283−293.
(23) Konopka, S. J.; McDuffie, B. Diffusion Coefficients of Ferri- and Ferrocyanide Ions in Aqueous Media, Using Twin-Electrode Thin-Layer Electrochemistry. *Anal. Chem.* **1970**, *42* (14), 1741−1746.
(24) Kaplan, M.; Kilic, T.; Guler, G.; Mandli, J.; Amine, A.; Ozsoz, M. A Novel Method for Sensitive MicroRNA Detection: Electropolymerization Based Doping. *Biosens. Bioelectron.* **2017**, *92*, 770−778.
(25) Shao, H.; Chung, J.; Lee, K.; Balaj, L.; Min, C.; Carter, B. S.; Hochberg, F. H.; Breakefield, X. O.; Lee, H.; Weissleder, R. Chip-Based Analysis of Exosomal mRNA Mediating Drug Resistance in Glioblastoma. *Nat. Commun.* **2015**, *6*, 6999.
(26) Yekula, A.; Minciacchi, V. R.; Morello, M.; Shao, H.; Park, Y.; Zhang, X.; Muralidharan, K.; Freeman, M. R.; Weissleder, R.; Lee, H.; et al. Large and Small Extracellular Vesicles Released By Glioma Cells in Vitro and in Vivo. *J. Extracell. Vesicles* **2020**, *9* (1), 1689784.
(27) Brennan, C. W.; Verhaak, R. G.; McKenna, A.; Campos, B.; Noushmehr, H.; Salama, S. R.; Zheng, S.; Chakravarty, D.; Sanborn, J. Z.; Berman, S. H.; et al. The Somatic Genomic Landscape of Glioblastoma. *Cell* **2013**, *155* (2), 462−477.
(28) Aldape, K. D.; Ballman, K.; Furth, A.; Buckner, J. C.; Giannini, C.; Burger, P. C.; Scheithauer, B. W.; Jenkins, R. B.; James, C. D. Immunohistochemical Detection of Egfrviii in High Malignancy Grade Astrocytomas and Evaluation of Prognostic Significance. *J. Neuropathol. Exp. Neurol.* **2004**, *63* (7), 700−707.
(29) Choe, J. H.; Watchmaker, P. B.; Simic, M. S.; Gilbert, R. D.; Li, A. W.; Krasnow, N. A.; Downey, K. M.; Yu, W.; Carrera, D. A.; Celli, A.; et al. Synnotch-Car T Cells Overcome Challenges of Specificity, Heterogeneity, and Persistence in Treating Glioblastoma. *Sci. Transl. Med.* **2021**, *13* (591), eabe7378.
(30) Sheehan, P. E.; Whitman, L. J. Detection Limits for Nanoscale Biosensors. *Nano Lett.* **2005**, *5* (4), 803−807.

https://doi.org/10.1021/acscentsci.1c01193
ACS Cent. Sci. 2022, 8, 110−117